4-21-2010

# Carbon Monoxide in Disks Around Two T Tauri Stars: RY Tau & DG Tau

Sammanani Shakya Premachandra
*University of Missouri-St. Louis*

# Carbon Monoxide in Disks

# Around Two T Tauri Stars: RY Tau & DG Tau

Sammanani Shakya Premachandra

Astrophysics Research Group
Department of Physics and Astronomy
University of Missouri – St. Louis

A Thesis Submitted to the Faculty at the University of Missouri – St. Louis
For the degree of Master of Science

May 2010

Advisory Committee

Dr. Erika Gibb

Dr. Bruce Wilking

Dr. Bob Henson

**Acknowledgements**

I would like thank Dr. Erika Gibb for her encouragement and guidance without which this endeavor would not have been successful.

I also would like to thank Daniel Blake, Kari Wojkowski, David Horne, Adam Scott, David Coss, Daisuke Takeshita and all other graduate students for their support at various junctures.

I am indebted to the department of Physics and Astronomy for the facilities and accommodating me in various ways.

Last but not least, I would like to thank my family for all the support they have given me throughout the Journey at UMSL.

## Contents



## List of Tables

## List of Figures

## Abstract

I present high-resolution, near infrared NIRSPEC spectra of carbon monoxide for two classical T Tauri stars: RY Tau and DG Tau. The purpose of the study is to further test whether there is a correlation between gas and dust with inclination to constrain models of dust settling and turbulence in disks. $^{12}$CO overtone and fundamental absorption lines in the 2.3 and 4.7 μm spectral region were measured, respectively. $^{13}$CO was detected for DG Tau. Rotational temperatures and column densities were calculated for each source. The ratio ~ $N_{CO}/A_V$ was measured as a function of inclination and compared to the results presented by Rettig et al. (2006). The results for RY Tau follow the trend reported by Rettig et al. (2006). The gas to dust ratio toward DG Tau is enormously larger than that found for similar sources.

## 1. Introduction

Star formation begins in dense concentrations of interstellar gas and dust called dark molecular clouds. These molecular clouds are low in density ~ $10^9$ $m^{-3}$, having temperatures of ~10K (Zeilik and Gregory, 1998). Star formation starts when the denser part of the cloud core collapses under its own gravity. Firstly, cores start to collapse and then the outer cloud. As the core collapses, the molecular cloud breaks into fragments, releasing gravitational potential energy as heat. As the temperature and pressure increase, these fragments form in to protostars. As the protostars form, the temperature and the pressure go up in the center of the protostar.

Young stellar objects (YSOs) are divided into different categories depending on their age, mass and environment. We are studying classical T Tauri stars, which are low mass young stars. T Tauri stars are pre-main sequence stars that are surrounded by disks. These disks contain gas and dust. They are mostly in between $10^5$ and $10^8$ years in age and have a low mass of 0.5 to 3.0 $M_\odot$. Evolution of YSOs can be categorized into four stages. Class 0 stage objects are young protostars which are surrounded by an envelope of dust and gas ~ $10^3$ to $10^4$ AU in size. These objects have ages of approximately $10^4$ years (Feigelson and Montmerle, 1999). As the YSO reaches the class I stage, conservation of angular momentum causes the envelope to flatten into a disk while decreasing the radius of the envelope. In this stage, most of the material has accreted onto the disk or the star. The YSOs start interacting with an accretion disk in class II stage giving rise to a classical T Tauri star. Class III, weak-emission T

Tauri stars have little or no accretion disks (Wolk & Walter, 1996; Feigelson and Montmerle, 1999). In this project we are interested in studying classical T Tauri stars. The study of the evolution of planetary systems helps us to understand the formation of planets since the planets form from the disks.

Carbon monoxide (CO) is the second most abundant molecule in disks next to $H_2$. Even though $H_2$ is the most dominant gas component in the circumstellar disks, it is difficult to detect. In contrast, the rovibrational lines of CO are strong over a range of column densities and temperatures, and can be used as a diagnostic to infer information about their environment (Brittain et al.2003; Najita et al.2003). The rotational temperature of CO can be used to infer the gas temperature in the disk, assuming the gas is thermalized.

Grain growth refers to the increase in the size of grains, probably by collisional sticking. This eventually leads to the formation of planetesimals through gravitational interaction (Dullemond & Dominik 2004). Dust settling and grain growth are expected to take place in the upper disk atmosphere (Miyake & Nagakawa 1995; Dullemond & Dominik 2004) until a balance with turbulence is reached towards the midplane (Rettig et al. 2006). Rettig et al. (2006) presented observations to test the extent to which dust preferentially settles to the midplane of the disk atmosphere. While the grain growth and dust settling will decrease the column density of particles at high disk latitude, it will increase the density towards the midplane (Rettig et al. 2006). To test this theory, Rettig et al. (2006) examined the gas-to-dust ratio for four

disks with known inclinations, ranging from nearly face-on to nearly edge-on. They found that dust-to-gas ratio decreased as inclination increased. If the dust and gas are well mixed in YSO disks (D'Alessio et al. 1999), it would be expected that the correlation between the column density and the extinction is independent of the viewing angle. If dust settles towards the midplane in YSO disks, face-on disk should be expected to have a larger ratio than a disk viewed edge on (Rettig et al. 2006). In the latter case, this ratio should approach the interstellar gas-to-dust ratio. The preliminary results of Rettig et al. (2006) indicated that dust settling or grain growth has occurred.

Recent models predict that dust particles settle towards the midplane (Garaud et al. 2004; Garaud & Lin 2004; Fouchet et al. 2005). The current question is: how are dust and gas mixed in the disk? Therefore, many sources need to be analyzed for a better understanding of how dust and gas are mixed. In this project, we investigated the gas/dust ratio in two additional classical T Tauri stars with known inclinations to compare with Rettig et al. (2006).

The observations, data reduction and analysis techniques are discussed in § 2. In § 3, I discuss the results for each source. The discussion and future work are discussed in § 4 and 5, respectively.

## 2. Data reduction and CO analysis

### 2. 1 Observations and Data Reduction

Data in this project were collected using the NIRSPEC instrument (McLean et al. 1998) at the W.M Keck Observatory on Mauna Kea, Hawaii. NIRSPEC is a near-infrared spectrometer, which provides a high resolving power ($\lambda/\Delta\lambda$) of ~ 25,000. Table 1 provides a summary of the K and M band observations. We targeted the fundamental and overtone absorption lines of carbon monoxide in the 4.7 μm (M) and 2.3 μm (K) regions, respectively. The data were gathered in an (A, B, B, A) sequence. This describes where the object is positioned in the slit of the NIRSPEC instrument, i.e., the upper or lower half of the slit. The data in this work were reduced using IDL (Interactive Data Language) routines. The correct order was chosen and the data were cropped from a 1024×1024 to a 1024×150 pixel area.

Table 1.

Observations

| Object | Date | Spectral Range($cm^{-1}$) | Setting | Integration Time(s) |
|---|---|---|---|---|
| | | K band | | |
| DG Tau | Feb 17 2006 | 4200-4265 | K1 | 720 |
| DG Tau | Feb 17 2006 | 4263-4323 | K2 | 240 |
| RY Tau | Feb 18 2006 | 4200-4265 | K1 | 480 |
| RY Tau | Feb 18 2006 | 4263-4323 | K2 | 240 |
| | | M band | | |
| DG Tau | Feb 18 2006 | 1986-2018 | M-wide | 240 |
| RY Tau | Feb 18 2006 | 1986-2018 | M-wide | 240 |

The data files were dark-subtracted and flat-fielded. This was done to account for pixel-to-pixel sensitivity variations and in order to remove hot or dead pixels. To clean the data, each pixel was compared with the nearby pixels and verified if it was within a selected standard deviation ($3\sigma$). The spatial and spectral dimensions were straightened before extracting the spectrum. The straightening procedure was made using a Gaussian fit on each of the 1024 columns and identifying the peaks of the A and B beams. Subtracting A and B beams, (A-B-B+A), the sky was cancelled to first order. The A beam collects the sky counts when the telescope in the B position and vice versa. Skylines due to $H_2O$ and CO display as vertical lines in the frame (Figure 1).

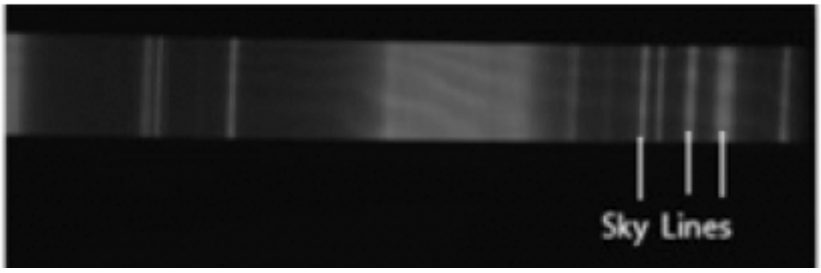


Figure 1. Sky lines are shown on an AB set in the M-wide band setting for a sample source.

Once the data were dark-subtracted, flat-fielded, cleaned, straightened, and sky subtracted, the Spectral Synthesis Program (Kunde and Maguire, 1974) and the updated HITRAN 2004 database (Rothman et al. 2005) were used to straighten the data spectrally. This was done in order to wavelength calibrate and remove skylines.

To stretch the data, the central wave number and dispersions (left and right) of the A and B beams were determined separately. The dispersion fitting has to be adequate in order to fit a proper atmospheric model. This was achieved by adjusting the stretch manually. i.e. defining right or left dispersion coefficients up to ninth order dispersions.

The telluric abundances were adjusted to fit the depths of the atmospheric absorptions. When comparing with other molecules, $H_2O$ mostly varies with time for the A and B beams. The sky background was found to be dominated by water and CO in the M-Wide setting.

The difference in counts between telluric lines in successive A and B beams should be close to zero. A figure of miscancelled sky is shown below (Figure 2). The miscancelled sky lines appear in beams mainly due to rapidly changing weather, i.e., thin clouds.


Figure 2. Miscancelled sky lines are shown on an AB set in the M-Wide setting for a sample source.

Therefore, to correct the appropriate data frame, a method that analyzed the background level was carried out to subtract the excess sky background (Figure 3).

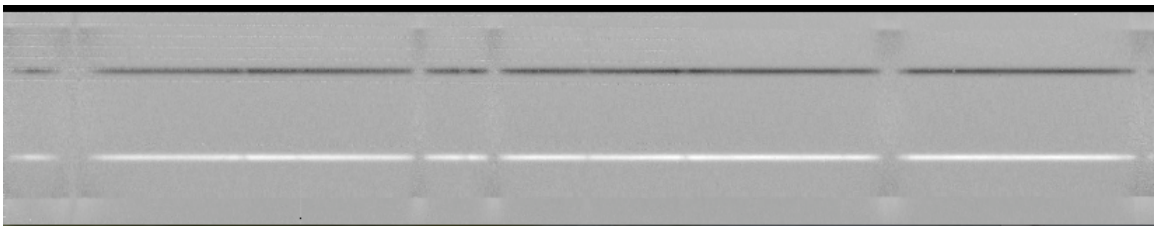

Figure 3. Data frame with the corrected sky background in the M-Wide band.

Finally, the A and B beam frequencies were interpolated to the same dispersion to get one spectrum. The telluric model was subtracted from the interpolated spectrum to get the residual plot. An example of the interpolated final spectrum with telluric model and residual plot is shown in Figure 4.

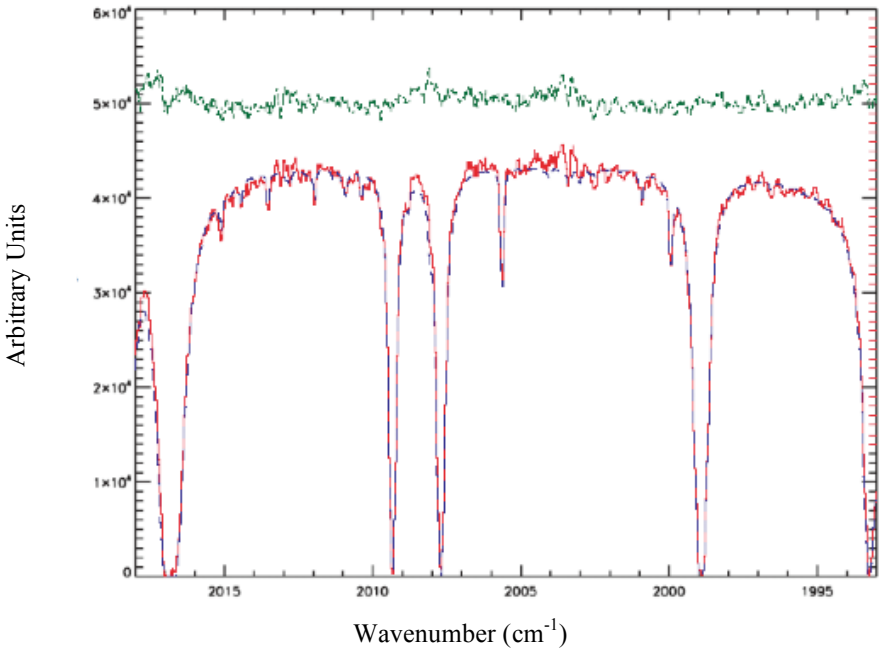


Figure 4. Illustrates the final spectrum for M band data from a sample source. Plotted with red, blue and green color lines are the extracted spectrum, telluric model and the residual, respectively.

## 2.2 Removal of photospheric lines

The spectra of Classical T Tauri stars have photospheric absorption lines superposed on CO absorption from the disk, particularly in the K band. Therefore, we applied NEXTGEN and Marcs advanced stellar photosphere models (Hauschildt 1999; Najita 2008) to the K band data to remove contamination. In order to do that, we compared our sources to spectroscopic standards of the same spectral type. The spectroscopic standards were corrected to the veiled level of each source

(Hesman & Gunther 1997). To accomplish a best fit for each model, the models were Doppler shifted to the data and compared to the original data by the least squares method (Horne et al. in prep). The preliminary residual plot for DG Tau before removing the photospheric lines is shown in Figure 5(a) and the final residual for DG Tau after removing photospheric lines is shown in Figure 5(b).

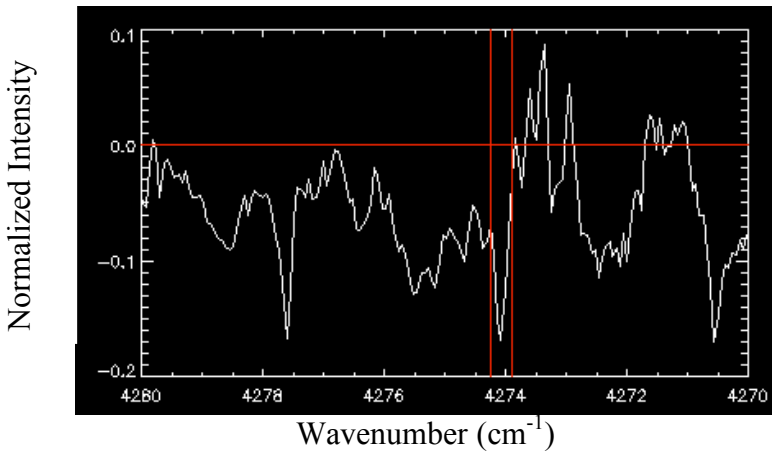


Figure 5(a). Indicates the residual plot of K2 Order 33 for DG Tau, before removing the photospheric lines. Two vertical lines in red color indicate the selected region of the absorption CO line.

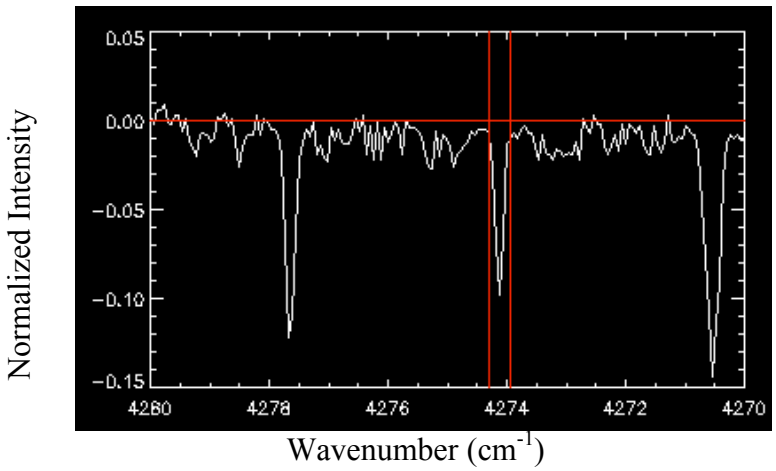


Figure 5(b). Indicates the residual plot of K2 Order 33 for DG Tau after removing the photopheric lines. Two vertical lines in red color indicate the selected region of the absorption CO line.

## 2.3 CO Analysis

Equivalent widths of the absorption line profiles were measured by fitting Gaussians to each absorption line and by directly integrating. This was done in order to measure the area of each CO line. We examined that both of the methods produced comparable values except in the case where an absorption line was blended with another feature. The CO lines have emissions superposed in the M band for RY Tau and DG Tau. A Gaussian profile was fitted to each side of the absorption lines to subtract the emissions. This was done in order to extract the absorption lines for the analysis.

The column densities and temperatures of the measured CO absorptions were determined with the help of Boltzmann's equation.

$$N_{J''} = (2J''+1)e^{-hcBJ''(J''+1)/kT}$$

$$N_{J''}/N_{tot} = (2J''+1)e^{-hcBJ''(J''+1)/kT} / Q \qquad (1)$$

where B is the rotational constant, J'' is the rotational quantum number of the lower state, h is Planck's constant, c is the speed of light, k is Boltzmann's constant, $N_{J''}$ is the population in each level and Q = kT/hcB is the total rotational partition function at the rotational temperature of the gas. Q is determined by using the general partition function, where the general partition function is given by:

$$Q_r = \sum (2J''+1)e^{-hcBJ''(J''+1)/kT} \quad \text{(Sum over J's)} \qquad (2)$$

Using asymptotic expansion, formula (2) can be written as,

$$Q_r = kT/hcB + 1/3 + hcB/15kT + 4/315(hcB/kT)^2 + \ldots\ldots \qquad (3)$$

For small B and large T, formula (3) goes over into the (classical) result

$$Q_r = kT/hcB \qquad \text{(Herzberg, 1950)} \qquad (4)$$

If the CO lines are optically thin, then the equivalent width is related to the column density by

$$N_{J''} = EW/\ 8.85 \times 10^{-13} \cdot f \qquad (5)$$

Where f is the oscillator strength of the absorption line and the constant is:

$$(\pi e^2 / mc^2)$$

The Boltzmann equation was modified to plot population diagrams with $\ln(N_{J''}/(2J''+1))$ vs $E_J/k$. Then the rotational temperature was determined by the negative inverse of the slope of the best-fit line.

The percent of the total molecule which should fall in one rovibrational state provides the measure of fractional population. The fractional population is determined by:

$$f_p = (2J''+1)\, e^{-hcBJ''(J''+1)/kT} / Q \qquad (6)$$

Then the total column density was calculated by:

$$N_{tot} = N_{J''}/\ f_p .$$

Once the temperatures and column densities were determined, we calculated gas-to-dust ratios for each source and compared our results to those obtained by Rettig et al. (2006). Using the temperature and the column density, we determined the ratio of $\sim [N(CO)/A_V]_{disk}$ for each source, where $A_V$ is the visual extinction (in magnitudes) due to dust. This value was compared to the interstellar ratio of $[N(CO)/A_V]_{interstellar} \sim 1.4 \times 10^{17}\ cm^{-2}\ mag^{-1}$. This interstellar ratio was obtained by the measured $CO/H_2$ ratio to

be $\sim 1.56 \times 10^{-4}$ and $A_V/N_{H2} \sim 10.8 \times 10^{-22}$ mag/cm$^2$ (Mathis 1990). Kulesa (2002) confirmed the ratio of $A_V/N_H$ up to $A_V = 60$.

Finally, we calculated the ratio of $[N(CO)/A_V]_{disk}/[N(CO)/A_V]_{interstellar} = \Delta$ for each source and compared to results by Rettig et al. (2006). Table 2 presents measurements for $^{12}$CO v=2-0, v=1-0 and $^{13}$CO v=1-0. The final results are shown in Table 3.

Table 2.

| Line ID | Rest | RY Tau | RY Tau |
|---|---|---|---|
| $^{12}$CO v: 2-0 | Wavenumber (cm$^{-1}$) | EW (x10$^{-3}$ cm$^{-1}$) | COLUMN DENSITY (cm$^{-2}$) |
| R0 | 4263.837 | 7±5 | (8.5±0.1)E+18 |
| R1 | 4267.541 | 11±5 | (6.2±0.2)E+18 |
| R3 | 4274.74 | 15±5 | (5.1±0.1)E+18 |
| R6 | 4285.008 | 24±10 | (6.2±0.3)E+18 |
| R15 | 4311.961 | 56±10 | (4.9±0.2)E+18 |
| R16 | 4314.596 | 12±2 | (1.4±0.3)E+19 |
| P1 | 4256.217 | 72±10 | (8.9±0.2)E+18 |
| P2 | 4252.302 | 19±5 | (1.2±0.2)E+18 |
| P12 | 4209.343 | 75±20 | (4.2±0.3)E+18 |
| $^{12}$CO v: 1-0 | | | |
| R0 | 2147.081 | 11±5 | (3.3±0.1)E+17 |
| R1 | 2150.855 | 77±10 | (1.1±0.2)E+17 |
| P1 | 2139.426 | 47±10 | (1.3±0.2)E+17 |
| P2 | 2135.546 | 11±5 | (1.5±0.1)E+17 |
| P3 | 2131.631 | 13±5 | (1.2±0.1)E+17 |
| P4 | 2127.682 | 15±5 | (1.1±0.1)E+17 |
| P5 | 2123.698 | 25±5 | (1.5±0.1)E+17 |
| P6 | 2119.68 | 23±5 | (1.0±0.1)E+17 |
| P29 | 2018.148 | 63±20 | (1.4±0.3)E+17 |
| P30 | 2013.352 | 35±10 | (3.0±0.1)E+17 |
| P31 | 2008.525 | 42±10 | (2.1±0.1)E+17 |
| P32 | 2003.667 | 71±30 | (3.0±0.1)E+17 |
| P33 | 1998.78 | 15±5 | (2.1±0.2)E+17 |

| Line ID | Rest | DG Tau | DG Tau |
|---|---|---|---|
| $^{12}$CO v: 2-0 | Wavenumber ($cm^{-1}$) | EW ($x10^{-3}cm^{-1}$) | COLUMN DENSITY($cm^{-2}$) |
| R0 | 4263.837 | 34±10 | (4.5±0.3)E+19 |
| R1 | 4267.541 | 15±5 | (1.1±0.5)E+19 |
| R3 | 4274.74 | 17±5 | (5.6±0.4)E+18 |
| R4 | 4278.234 | 18±5 | (5.8±0.2)E+18 |
| R5 | 4281.657 | 19±5 | (5.6±0.4)E+18 |
| R6 | 4285.008 | 7±5 | (2.1±0.6)E+18 |
| R10 | 4297.704 | 19±5 | (6.2±0.5)E+18 |
| R11 | 4300.699 | 21±10 | (7.5±0.3)E+18 |
| R12 | 4303.623 | 14±10 | (6.0±0.3)E+18 |
| R13 | 4306.475 | 16±5 | (8.2±0.6)E+18 |
| R14 | 4309.254 | 54±20 | (3.2±0.3)E+18 |
| R15 | 4311.961 | 11±5 | (8.5±0.1)E+18 |
| R16 | 4314.596 | 18±5 | (1.7±0.3)E+19 |
| R18 | 4319.648 | 17±5 | (2.8±0.5)E+19 |
| P1 | 4256.217 | 67±30 | (9.1±0.2)E+19 |
| P2 | 4252.302 | 89±50 | (6.3±0.7)E+19 |
| P3 | 4248.317 | 14±2 | (2.0±0.4)E+19 |
| P4 | 4244.263 | 79±40 | (3.2±0.5)E+19 |
| P6 | 4235.946 | 76±40 | (2.6±0.4)E+19 |
| P7 | 4231.685 | 38±10 | (1.3±0.2)E+19 |
| P8 | 4227.354 | 36±10 | (1.2±0.6)E+19 |
| P9 | 4222.954 | 14±5 | (5.1±0.8)E+18 |
| P11 | 4213.948 | 56±30 | (2.5±0.3)E+19 |
| P12 | 4209.343 | 34±10 | (1.8±0.7)E+19 |
| P13 | 4204.669 | 34±10 | (2.4±0.6)E+20 |
| $^{12}$CO v: 1-0 | | | |
| R0 | 2147.081 | 110±10 | (4.4±0.2)E+18 |
| R1 | 2150.855 | 120±10 | (1.7±0.6)E+18 |
| P1 | 2139.426 | 70±50 | (2.0±0.3)E+18 |
| P2 | 2135.546 | 110±10 | (8.0±0.4)E+17 |
| P6 | 2119.68 | 110±10 | (6.3±0.2)E+17 |
| P29 | 2018.148 | 79±10 | (1.5±0.3)E+18 |
| P30 | 2013.352 | 5±1 | (1.2±0.4)E+18 |
| P32 | 2003.667 | 51±10 | (1.7±0.6)E+18 |
| $^{13}$CO v: 1-0 | | | |
| R10 | 2134.313 | 19±10 | (7.1±0.2)E+16 |
| R12 | 2140.827 | 62±30 | (7.1±0.2)E+16 |
| R13 | 2144.033 | 22±10 | (8.7±0.2)E+16 |
| R15 | 2150.34 | 16±10 | (6.9±0.2)E+16 |

## 3. Results

Table 3 reports the results for $^{12}CO$ fundamental and overtone absorption lines for two additional sources with the results for four other sources presented by Rettig et al. (2006).

### RY Tau

RY Tau is a classical T Tauri star located in the Taurus-Auriga cloud, where d = 140 pc (Elias, 1978; Amboage et al 2008). It has a spectral type of F8-G1 (Mora et al.2001; Calvet et al.2004; Scherergerer et al. 2007; Amboage et al. 2008) and a stellar mass of 1.69 $M_{\odot}$ (Beckwith et al. 1990; Scherergerer et al. 2007) with a stellar luminosity of 12.8 $L_{\odot}$ (Akeson et al. 2005). The disk inclination was found to be 25˚ (Koerner et al. 1995) with a visual extinction of $A_V \sim (2.2 \pm 0.2)$ mag (Calvet et al. 2004; Scherergerer et al. 2007).

Preliminary results of RY Tau specify that the carbon monoxide absorption has a rotational temperature of approximately 260±40 K from the K band data. The fundamental $^{12}CO$ absorption lines in the M band spectrum shown in Figure 6, are optically thick. Using the K band data, the column density of $^{12}CO$ was calculated to be $\sim 2.8 \pm 0.1 \times 10^{18}$ $cm^{-2}$. Similarly, using the M band data, the column density was calculated to be $\sim 1.7 \pm 0.1 \times 10^{17}$ $cm^{-2}$. The calculated rotational temperature and the column density for the M band data do not agree within the errors when compared to the K band data. Therefore, we can conclude the M band data is optically thick. All population diagrams for RY Tau are shown in Figure 8. K band data indicate the ratio

between the column density and the extinction is, $[N(CO)/A_V]_{disk} \sim 1.3\pm0.2\times10^{18}$ cm$^{-2}$ mag$^{-1}$. Therefore, the calculated $\Delta = 9.2\pm0.1$, which is consistent with the results reported by Rettig et al. (2006). This result suggests that dust settling and/or grain growth has occurred.

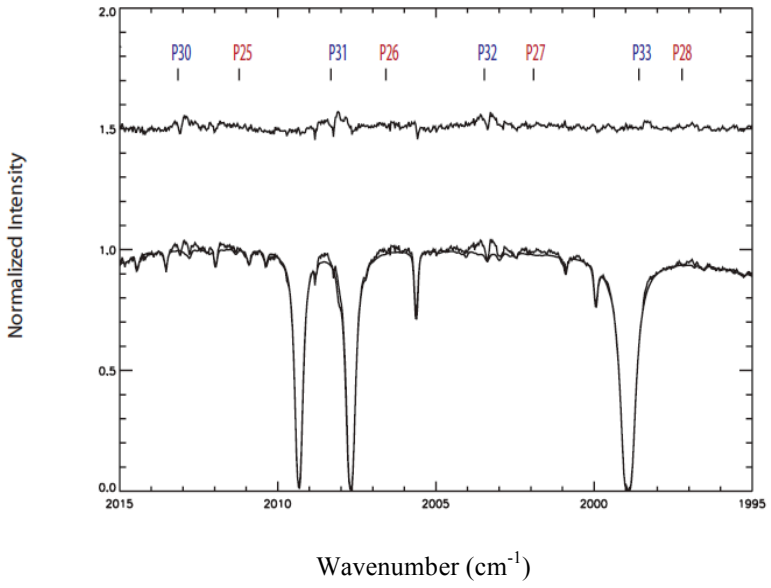


(a) M-Wide Order 15

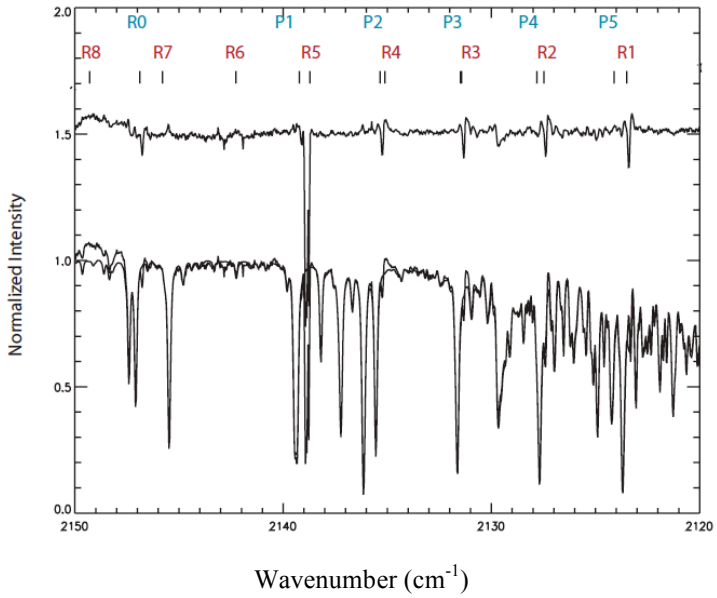


(b) M-Wide Order 16

Figure 6. Indicates the normalized plot of RY Tau for the M band data. The spectrum is plotted with the solid line, the telluric model with the dashed line and the residual (spectrum-telluric) is shown above the spectrum and telluric model. Rovibrational line positions for $^{12}$CO v=1-0 and v=2-1 are marked and identified in blue and red color, respectively.

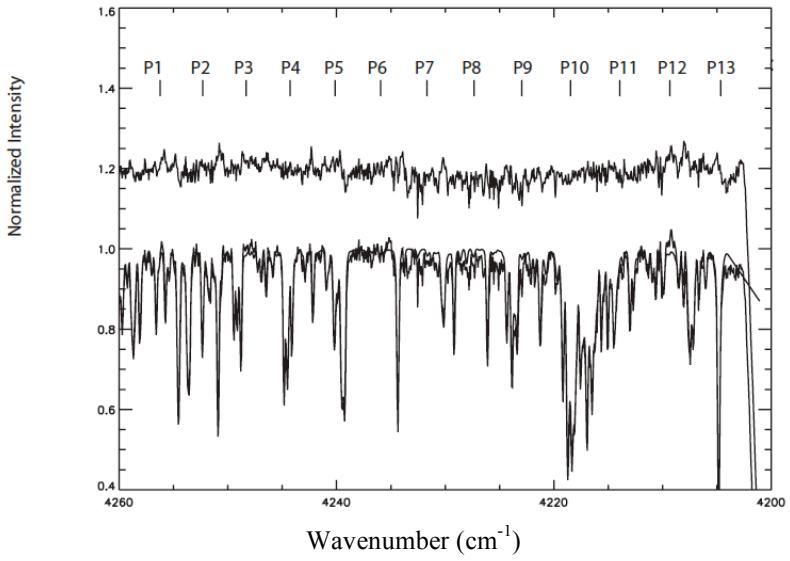


(a) K1 Order 32

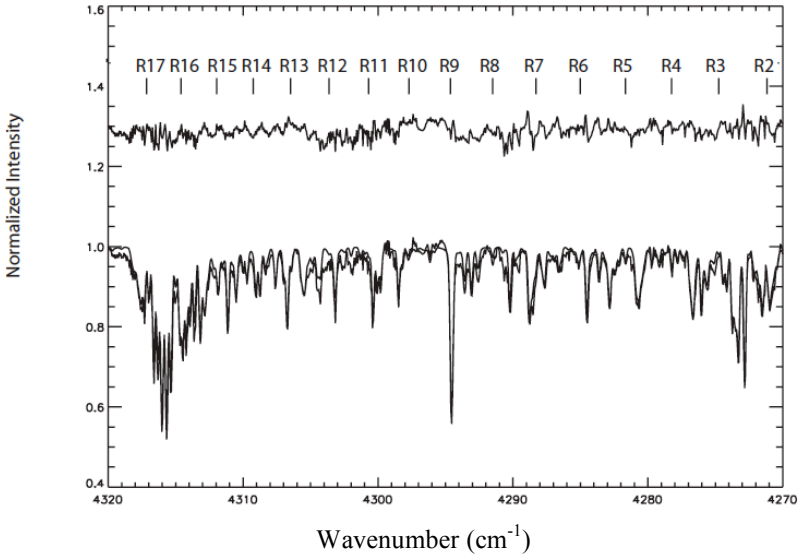


(b) K2 Order 33

Figure 7. Normalized spectrum of RY Tau for the K band data. The spectrum is plotted with the solid line, the telluric model with the dashed line and the residual (spectrum-telluric) is shown above the spectrum and telluric model. Rovibrational line positions are shown in the graph.

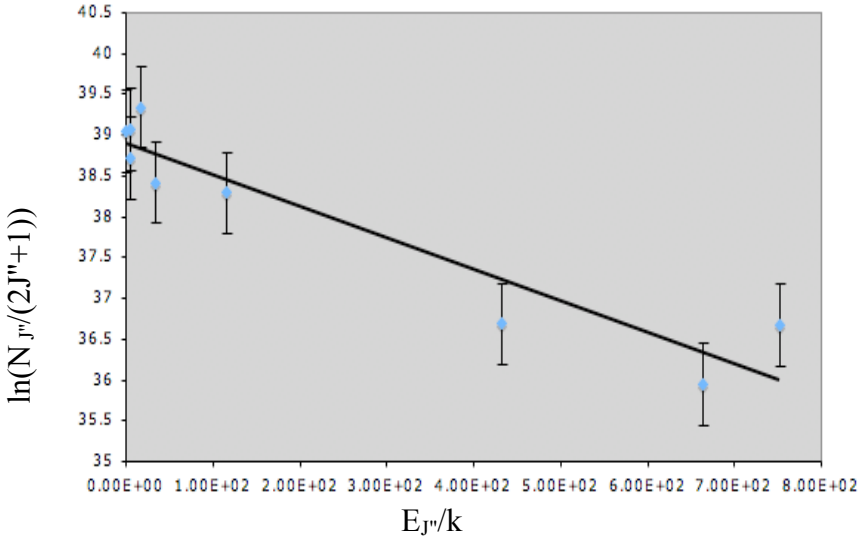


(a) K band $^{12}$CO with $T_{rot}$ = 260±40 K and $N_{CO}$ = 2.8±0.1×10$^{18}$ cm$^{-2}$

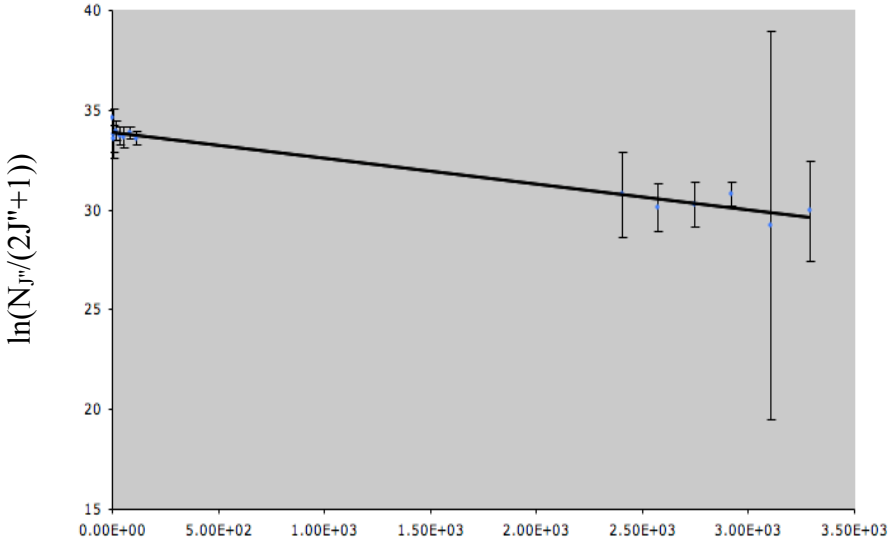


(b) M-Wide $^{12}$CO with $T_{rot}$ = 760±35 K and $N_{CO}$ = 1.7±0.1×10$^{17}$ cm$^{-2}$

Figure 8. Population diagram for CO for RY Tau data.

## DG Tau

DG Tau is a classical T Tauri star, which is located in the Taurus molecular cloud and at a distance of 140 pc (Elias 1978;Kitamura et al. 1996). Estimated spectral types range from K5 to M2 (Hartigan et al. 1995). It has a K magnitude of 6.98 ± 0.013 (Colavita et al. 2003) and a disk inclination of 70˚±10˚ (Kitamura et al. 1996;Colavita et al. 2003). The mass and the luminosity of the star are estimated to be 0.56 $M_{\odot}$ and 1.7 $L_{\odot,}$ respectively (Beckwith et al. 1990; Kitamura et al. 1996). The visual extinction was found to be $A_V \sim 1.6$ (Kitamura et al. 1996; Adams et al. 1990; Beckwith et al. 1990).

Before removing photospheric lines, preliminary results for DG Tau, indicated that the CO has a rotational temperature of $T_{rot} \sim 860$ K in the K band data. Figure 8 and 9 show the spectra for each order. After removing photospheric absorption from the K band data, it resulted a rotational temperature of 290±60 K and a column density of $3.7\pm0.1\times10^{19}$ $cm^{-2.}$ Using the M band the column density was calculated to be $9.2 \pm0.5\times10^{17}$ $cm^{-2}$, which suggest the M band is optically thick. $^{13}CO$ was detected in the M band and resulted in a rotational temperature and column density of 714±40 K and $7.4\pm0.2\times10^{16}$ $cm^{-2}$, respectively. However, the results of $^{13}CO$ do not agree with the results obtained from $^{12}CO$. The reason for the discrepancy of $^{13}CO$ is may be due to not having sufficient quality data to obtain a realistic rotational temperature and column density. All population diagrams are shown in Figure 11. The obtained ratio between the column density and the visual extinction $[N(CO)/A_V]_{disk} \sim 2.3\pm0.2\times10^{19}$ $cm^{-2}$ $mag^{-1}$ and $\Delta = 164\pm10$ is much higher than the

result reported by Rettig et al. (2006). However, DG Tau does not follow the trend on inclination and the extinction compared to other five sources in Table 3. This may be due to inadequately constrained orientation or an underestimate of the extinction ($A_V$) by ignoring scattering.

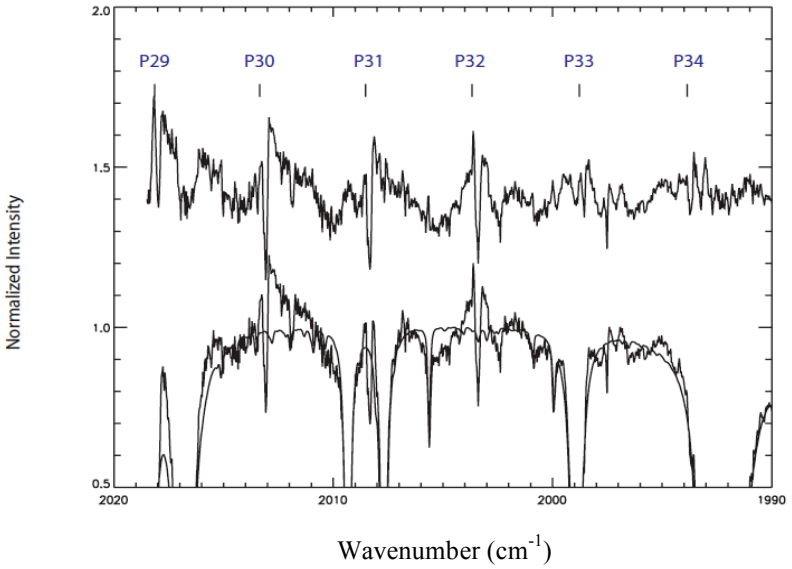


(a) M-Wide Order 15

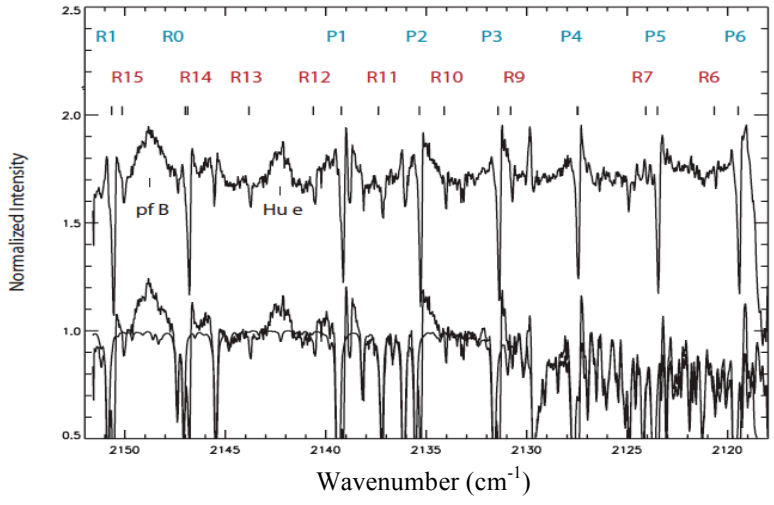


(b) M-Wide Order 16

Figure 9. Indicates the normalized plot of DG Tau for the M band data. The spectrum is plotted with the solid line, the telluric model with the dashed line and the residual (spectrum-telluric) is shown above the spectrum and telluric model. Rovibrational line positions for $^{12}CO$ and $^{13}CO$ are marked and identified in blue and red color, respectively.

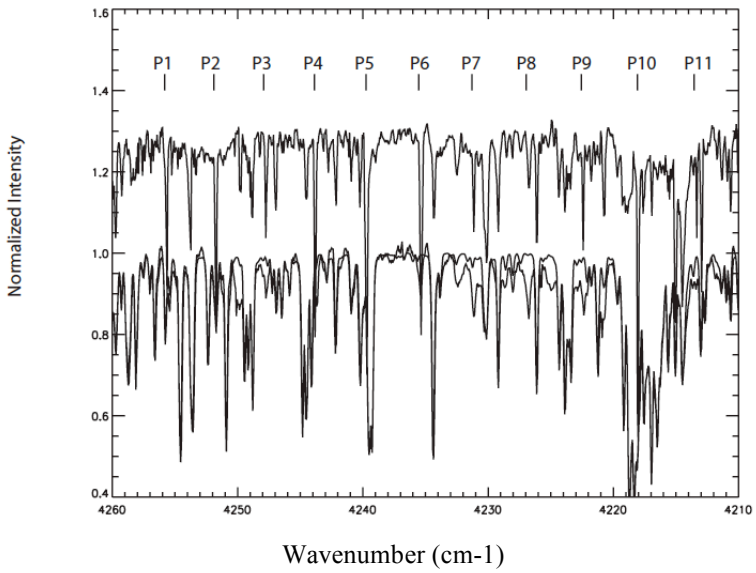


(a) K1 Order 32

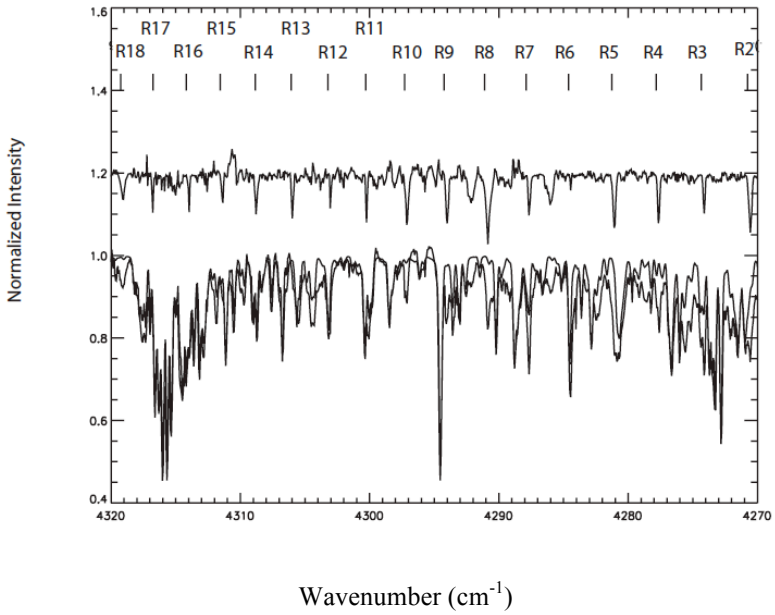


(b) K2 Order 33

Figure 10. Indicates the normalized plot of DG Tau for the K band data. The spectrum is plotted with the solid line, the telluric model with the dashed line and the residual (spectrum-telluric) is shown above the spectrum and telluric model. Rovibrational line positions are shown in the graph.

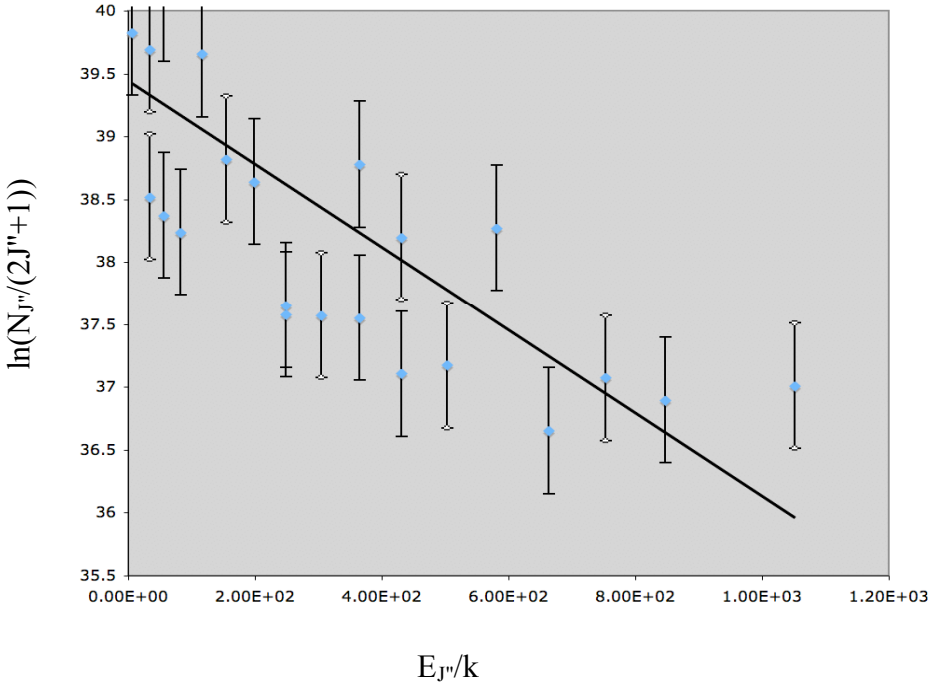


(a) K band $^{12}CO$ with $T_{rot} = 290\pm60$ K and $N_{CO} = 3.7\pm0.1\times10^{19}$ cm$^{-2}$

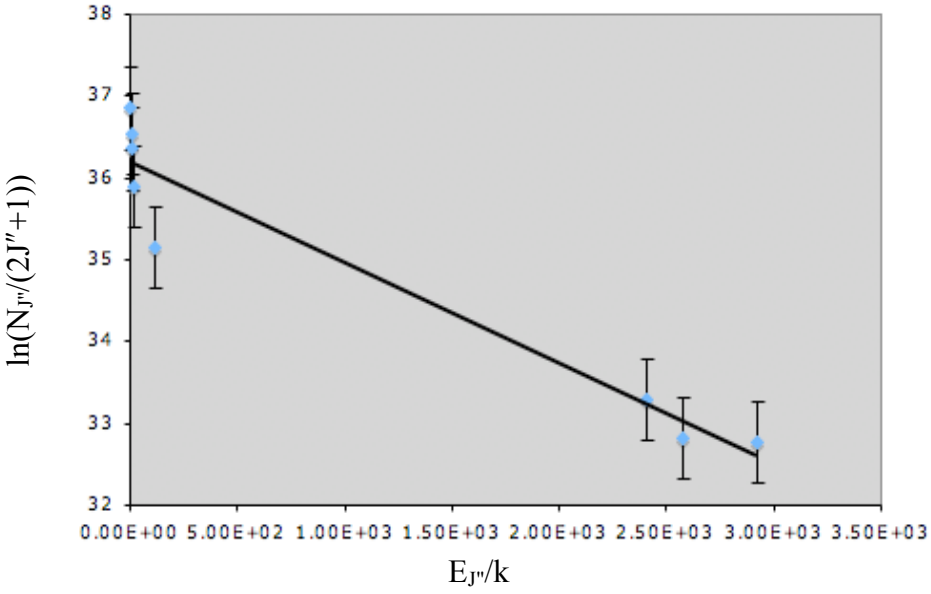


(b) M-Wide $^{12}CO$ with $T_{rot} = 830\pm30$ K and $N_{CO} = 9.2\pm0.5\times10^{17}$ cm$^{-2}$

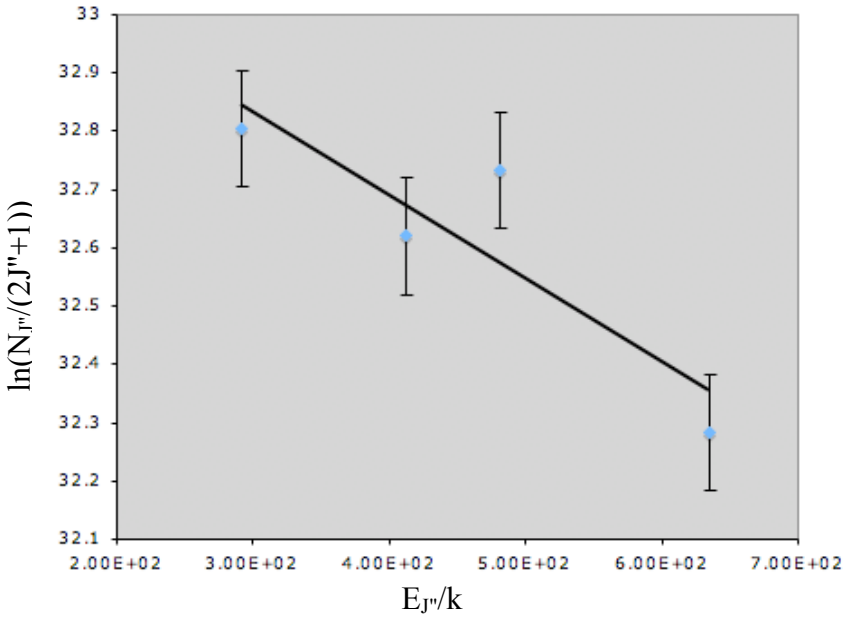


(c) M-Wide $^{13}CO$ with $T_{rot}$ = 714±40 K and $N_{CO}$ = 7.4±0.2×$10^{16}$ $cm^{-2}$

Figure 11. Population diagrams of CO for DG Tau data.

## 4. Discussion

The data were collected using M and K filters to target the fundamental (v=1-0) and overtone (v=2-0) lines of CO, respectively. The results of the two sources: RY Tau and DG Tau were compared to results reported by Rettig et al. (2006) to further test the dust stratification of the disks. Rotational temperatures and column densities of each source were compared along with the $N_{CO}/A_V$ and inclination. The sources showed a trend between inclination and $N_{CO}/A_{V,}$ which clearly suggests that dust settling and grain growth has occurred.

As we discussed, gas to extinction ratio is dominated by the effect of dust settling and grain growth. But this may not be the only ongoing effect. There could be additional issues to be counted. One of them could be the age difference among the sources we used in this project. It may effect gas-to-dust ratio. Another reason could be the differences in stellar masses, which may lead to differences in evolutionary timescales (Rettig et al. 2006).

(Kamp & Dullemond, 2004) modeled the gas and dust temperatures in the disk atmosphere as a function of scale height. If $T_{gas} > T_{dust}$, the scale height for the gas distribution relative to the dust distribution might affect the gas-to-dust ratio. This could be one of the reasons that DG Tau (~ 290 K) does not fit with the trend presented by Rettig et al. (2006). Inclination for DG Tau was assumed to be 70˚±10˚. Therefore, the reason for a discrepancy may be due to inadequately constrained orientation and this may indicate DG Tau has a slightly more face on orientation than

thought before. Also an underestimate of the extinction could be another reason for a discrepancy. Some groups have developed theoretical models to discuss the disk structure and the evolution of the disk (Goldreich & Ward 1973; Youdin & Chiang 2004). Balsara et al. (2009) tested the effect on gas-to-dust scale heights with different grain sizes as a function of time using 0.3 and 10 AU. They found that three different families of grains nearly overlap at 0.3AU. This may indicate dust and gas are well mixed in the disk atmosphere within a few orbits.

Table 3.

| Source | Inclination (deg) | $A_V$ | $[N(CO)/A_V]_{disk}$ ($cm^{-2}mag^{-1}$) | T(CO) (K) | Δ |
|---|---|---|---|---|---|
| RY Tau | 25 | 2.2±0.2 | $1.3\pm0.2 \times 10^{18}$ | 260±40 | 9.2±0.1 |
| T Tau N ∗ | 25-45 | 1.5 | $1.2\pm0.2 \times 10^{18}$ | ~ 100 | 8.1±1.5 |
| RNO 91∗ | 60±10 | 9 | $3.8\pm0.7 \times 10^{17}$ | ~ 50 | 2.7±0.5 |
| HL Tau∗ | 67±10 | 24 | $3.2\pm0.5 \times 10^{17}$ | ~ 100 | 2.3±0.4 |
| DG Tau | 70±10 | ~ 1.6 | $2.3\pm0.2 \times 10^{19}$ | 290±60 | 164±10 |
| T Tau S∗ | >80 | 35 | $2.6\pm0.4 \times 10^{17}$ | 100-300 | 1.8±0.4 |

∗Rettig et al. (2006), $A_V$ for RY Tau (Calvet et al. 2004; Scherergerer et al. 2007), $A_V$ for DG Tau (Kitamura et al. 1996; Adams et al. 1990;Beckwith et al. 1990). Disk inclination for RY Tau (Koerner et al. 1995). Inclination for DG Tau (Kitamura et al. 1995; Colavita et al. 2003)

## 5. Future work

Two additional sources are not sufficient to test the structure of the dust in disks. Therefore in the future, the number of sources should be increased in order to do a better analysis.

If CO lines cannot be fit with a straight line in a population diagram, this implies that the gas is optically thick. The CO lines for the M band were found to be optically thick and often superposed on broad CO emission lines originating in the hot inner disk. Therefore, we need to subtract a Gaussian profile from the emission lines to extract the absorption lines. Then we need to correct the equivalent width to correct for optical depth using a curve-of-growth analysis. As the dust becomes optically thick, the column density of CO is underestimated since you are not searching as far into the disk. In optically thick case, column density is given by,

$$N = (m_e c \varepsilon_0 / e^2) (\nu b \tau / f),$$

Where $\tau$ is the optical depth, $\nu$ is the wavenumber of the transition, b is the rms (root mean square) line width and b is given by, $b=\sigma_{rms}/1.665$ (Hobbs, 2005).
Since CO absorption lines are not resolved we cannot measure b directly. Therefore, we solve its value by taking R and P branches into account individually. i.e. R1 and P1 should result in same column density since they probe from the same energy level.

Better constraints will be used for the evolutionary state of each source and since better inclination determination will become available for some sources (Rettig et al. 2006), updates will be made to the list. Therefore, this will be approached with further observations (Horne et al. in prep). Also, using a larger sample will help to account for evolutionary differences of the sources.

REFERENCES

Adams, F. C., Emerson, J. P., and Fuller, G. A., 1990, ApJ, 357, 606

Akeson, R. L., Boden, A. F., Monnier, J. D., Millan-Gabet, R., Beichman, C., Beletic, J., Calvet, N., Hartmann, L., Hillenbrand, L., Koresko, C., Sargent, A., and Tannirkulam, A., 2005, ApJ, 635, 1173

Amboage, V.A., Dougados, C., Cabrit, S., Garcia, J.V., and Ferruit, P., 2008 A&A 493, 1029

Balsara, D. S., Tilley, David A., Rettig, T., and Brittain, S. D., 2009MNRAS. 397, 24

Beckwith, S. V. W., Sargent, A. I., Chini, R. S., and Guesten, R., 1990, AJ, 99, 924

Brittain, S. D., Rettig, T. W., Simon, T., Kulesa, C., Disanti, M. A., and Dello R. N., 2003, ApJ, 588, 535

Brittain, S. D., Rettig, T. W., Simon, T., and Kulesa, C., 2005,ApJ, 626, 283

Calvet, N., Muzerolle, J., Briceño, C., Hernández, J., Hartmann, L., Saucedo, J., and Gordon, K.D., 2004, AJ, 128, 1294

Colavita, M., Akeson, R., Wizinowich, P., Shao, M., Acton, S., Beletic, J., Bell, J., Berlin, J., Boden, A., Booth, A., and 53 coauthors., 2003 , ApJ, 592, 83

D'Alessio, P., Calvet, N., Hartmann, L., Lizano, S., and Cantó,J., 1999, ApJ, 527, 893

Dullemond, C. P., & Dominik, C., 2004, A&A, 421, 1075

Elias, J.H., 1978, ApJ, 224, 857

Feigelson, E.D., and Montmerle, T., 1999, ARA&A, 37, 363

Fouchet, T., Bézard, B., and Encrenaz, T., 2005, SSRv, 119, 123

Garaud, P., Barrière-Fouchet, L., and Lin, D. N. C., 2004, ApJ, 603, 292

Garaud, P., and Lin, D. N. C., 2004, ApJ, 608, 1050

Goldreich, P., Ward, W.R., 1973, ApJ, 183, 1051

Hartigan P., Edwards, S and Ghandour L., 1995, ApJ, 452, 736

Hessman, F. V., and Guenther, E. W., 1997, A&A, 321, 497

Hobbs, L.M., 2005MNRAS, 359, 1356

Herzberg, G., 1950, spectra of Diatomic Molecules (New York:Van Nostrand Reinhold), 370

Kamp, I., and Dullemond, C. P., 2004, ApJ, 615, 991

Koerner, D. W., and Sargent, A. I., 1995, AJ, 109, 2138

Kulesa C., 2002, Ph.D. thesis, Univ.Arizona

Kunde, V. R., and Maguire, W. C., 1974, JQSRT, 14, 803

Kitamura, Y., Kawabe, R., and Saito, M., 1996, ApJ, 465, 137

Mathis, J. S., 1990, ARA&A, 28, 37

McLean, I. S., et al., 1998, Proc, SPIE, 3354, 566

Mora, A., Merín, B., Solano, E., Montesinos, B., de Winter, D., Eiroa, C., Ferlet, R., Grady, C. A., Davies, J. K., Miranda, L. F., and 12 coauthors., 2001, A&A, 378, 116

Miyake, K., and Nakagawa, Y., 1995, ApJ, 441, 361

Najita, J., Carr, S., and Mathieu, R. D., 2003, ApJ, 589, 931

Najita, J. R., Crockett, N., and Carr, J. S., 2008, ApJ, 687, 1168

Pringle, J. E., 1981, ARA&A, 19, 137

Rettig, T., Brittain, S., Simon, T., Gibb, E., Balsara, D. S., Tilley, D. A.; Kulesa, C., 2006, ApJ, 646, 342

Rothman, L. S., Jacquemarta, D., Barbeet, A.., and 27 colleagues, 2004, J. Quant.Spec. Radiant. Transf, 96, 139

Schegerer, A. A., Wolf, S., Ratzka, T., and Leinert, C., 2007, A&A, 478, 779

Youdin, A. N., and Chiang, E. I., 2004, ApJ, 601, 1109Y

Wolk, S. J., and Walter, F. M., 1996, AJ, 111, 2066

Zeilik, M., and Gregory, S., Astronomy & Astrophysics fourth edition ( Fort Worth: Saunders College Publishing), 305